High-current-density field emitters based on arrays of carbon nanotube bundles

Harish M. Manohara, Michael J. Bronikowski,[a] Michael Hoenk,
Brian D. Hunt, and Peter H. Siegel
Jet Propulsion Laboratory, California Institute of Technology, 4800 Oak Grove Drive, Pasadena, California 91109

(Received 16 September 2004; accepted 29 November 2004; published 5 January 2005)

We have developed high-current density field emission sources using arrays of multiwalled carbon nanotube bundles. The field emission behavior of a variety of lithographically patterned array geometries was investigated and the arrays of 1-μm and 2-μm-diameter nanotube bundles spaced 5 μm apart (edge-to-edge spacing) were identified as the most optimum combination, routinely producing 1.5–1.8 A/cm^2 at low electric fields of approximately 4 V/μm, rising to $>$6 A/cm^2 at 20 V/μm over a $\sim$100-μm-diameter area. We have found that the field emission performance depends strongly on the bundle diameter and interbundle spacing and such arrays perform significantly better in field emission than ordered arrays of isolated nanotubes or dense, continuous mats of nanotubes previously reported in literature. © *2005 American Vacuum Society.*
[DOI: 10.1116/1.1850103]

I. INTRODUCTION

Carbon nanotubes (CNTs) have many exceptional properties that make them attractive for a variety of applications. In particular, past works[1–3] have shown that CNTs can have outstanding electrical field emission properties, with high emission currents at low electric field strengths (turn-on voltage as low as 1–3 V/μm and emission current as high as 0.1 mA from a single nanotube).[2,4] Carbon nanotubes are therefore attractive as cold-cathode field emission sources, especially for applications requiring high-current densities (hundreds to thousands of amperes per cm^2) and lightweight packages (high frequency vacuum tube sources).[5,6] However, it is also well known that the high emission capability of a single nanotube does not necessarily translate directly into high emission magnitudes from a larger area sample containing many such nanotubes because of the electrostatic screening effect. Past publications have reported current densities from CNT of 100–500 mA/cm^2 over areas on the order of 100 μm$\times$100 μm.[7–10] While Nilsson *et al.* have shown through simulations that the optimum nanotube packing density with best field penetration occurs when the intertube spacing is at least twice that of the nanotube height,[11] Suh *et al.* have shown through measurements that it is when the intertube spacing is equal to the nanotube height.[12] More recently, there have been many fundamental works on field emission optimization from CNTs using sparse, dense and patterned arrays of either forests or individual, vertically-aligned nanotubes or nanofibers.[13–17] But, achieving high-current densities (hundreds to thousands of amperes per square centimeter) over large nanotube sample areas with repeatability and emission longevity still remains an open problem.

As part of our efforts to develop a high-current-density electron source for a specifically targeted application, we have investigated the field emission behavior of CNT arranged in a variety of geometries. This work concerns itself with developing optimum array architectures of CNT field emitters that produce high emission densities (few amperes per sq. cm) at low electric fields (few V/μm) over a designed circular area of 100 μm diameter. After performing benchmark tests using continuous films of CNT of different densities and samples with isolated, individual CNT, we found that the best field emission (highest current and/or lowest required electric field) is achieved when the CNT are arranged in bundles of few microns in diameter, with the bundles arranged in arrays with an array spacing of several microns. We have studied the field emission characteristics of arrays of such CNT bundles, and have optimized field emission with respect to bundle size and separation. Interestingly, this optimization exhibited no direct or obvious conformity to the optimum emission geometries previously published in literature.[11,12]

II. EXPERIMENT

Our CNT are grown in a tube furnace, which contains a pressure-regulated 2-in.-diameter quartz tube. The CNT are grown on catalyst-coated substrates under a flowing mixture of ethylene and hydrogen. Typical CNT growth conditions are: C_2H_4 flow, 380 sccm; H_2 flow, 190 sccm; total pressure, 200 Torr; Temperature, 650 °C; growth time, 15 min. Our substrates consist of silicon wafers with a 400 nm layer of thermal silicon oxide (SiO_2). These substrates were patterned with a thin film, approximately 10 nm thick, of sputtered iron catalyst using electron beam lithography and lift-off processing, and then inserted into the tube furnace for CNT growth. Under these conditions, CNT will grow upon the

[a]Author to whom correspondence should be addressed; electronic mail: Michael.J.Bronikowski@jpl.nasa.gov

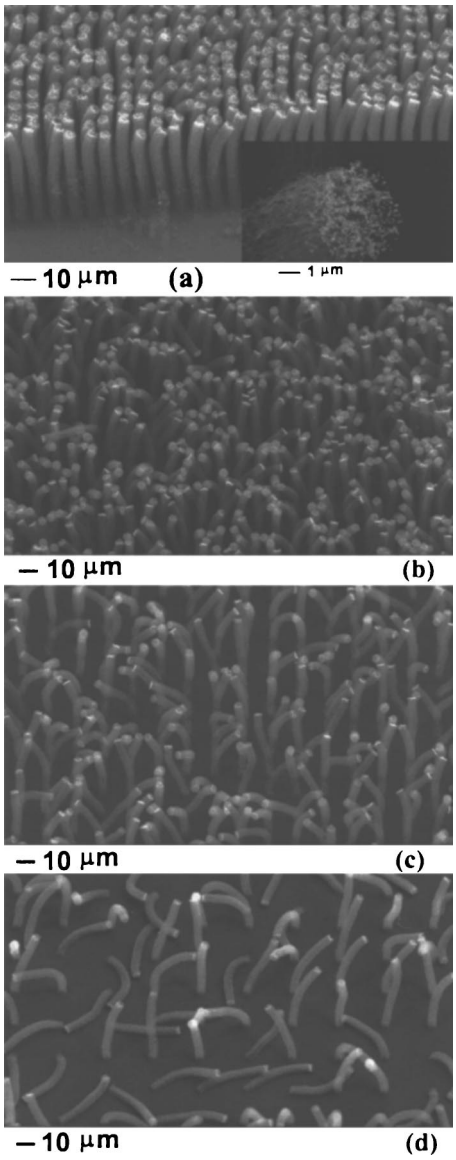

FIG. 1. SEM micrographs of carbon nanotube bundles grown from an array of 5-μm-diameter dots of iron catalyst, with various edge-to-edge spacings. The bundles shown in (a)–(d) are of 2 μm, 5 μm, 10 μm, and 20 μm edge-to-edge spacings, respectively. The inset of (a) shows a close-up of one nanotube bundle in which the individual nanotubes are visible. These micrographs show the degree of stiffness of CNT bundles as the interbundle spacing increases. The bundles droop significantly as the array spacing increases.

substrates only in the areas patterned with Fe catalyst. Typical CNT length was 50 μm$\pm$2 μm, while typical diameter of individual CNT was 10–20 nm.

The iron catalyst was patterned in square arrays consisting of circular dots with various diameter (in the range of 0.2–5.0 μm) and separation (in the range of 2–100 μm). These dots were typically written in arrays with size ranging from 500 μm to many millimeters. Figure 1 shows examples of CNT grown from arrays of 5-μm-wide dots of Fe catalyst with various catalyst dot spacing. The inset in Fig. 1(a) shows a close-up of one nanotube bundle in which the individual nanotubes are visible. We find that, for catalyst dots greater than 0.5 μm in size and greater than 2 μm edge-to-edge spacing, the growing nanotubes will stick together and form these cohesive, ropelike structures, whereas the CNT from smaller catalyst dots do not form bundles, but rather grow individually and tend to form low, bush-like structures. Evidently, there is a minimum size and spacing for a "patch" of growing CNT below which the nanotubes do not have enough mutual cohesion or restriction of space to form cohesive structures of roughly parallel CNT. The nanotube bundles exhibited sufficient mechanical strength to stand upright in closely spaced arrays (arrays of 2 μm, 5 μm, and 10 μm edge-to-edge spacings), but drooped in arrays of larger spacings (20 μm, 50 μm, and 100 μm), as illustrated in Fig. 1. Also, the degree of stiffness depended on the bundle diameter—larger bundles drooped lesser compared to smaller bundles for a given interbundle spacing, as illustrated in Fig. 2.

A schematic diagram of one of the array patterns that was used for field emission testing is shown in Fig. 3. Dots with diameters of 5 μm, 2 μm, 1 μm, 0.5 μm, and 0.2 μm were written in arrays of size 0.5 mm$\times$20 mm. Six such arrays were written for each dot size, with six different edge-to-edge spacing between dots: 100 μm, 50 μm, 20 μm, 10 μm, 5 μm, and 2 μm. By scanning a probe anode across these arrays, a comparative field emission behavior from different array combinations was investigated. In the discussion below, we confine our analysis to samples with this particular arrangement of CNT bundles, although, three different samples of similar or alternate CNT pattern were prepared and measured, and all gave qualitatively similar behavior of field emission with respect to CNT bundle size and spacing as described in paragraphs below.

The measurements were conducted using a flat-bottomed tungsten probe anode of 100 μm tip diameter. This tip was chosen to keep the area of field emission measurements consistent with the targeted application requirement. The anode was fixed to a *XYZ* micrometer stage to allow for scanning during measurements. Each array sample was mounted on a flat ceramic block and placed inside a high vacuum chamber. The anode-cathode gap was set to $\sim$15 μm considering an estimated full height of the nanotubes under the effect of the field. (At the selected gap, the area of field influence is restricted to that directly beneath the tip. This allows the estimation of the emission current density by approximating the emission area to be the same as the collection area, that is, the tip area of the anode probe.) The scan coordinate convention is shown in Fig. 3. Three lateral scans across the arrays (along *Y*) were conducted at three different longitudinal locations (in *X*) separated by at least 1 mm. The vacuum during measurements was typically from 1 to 7×10^{-5} Pa (1 to 5×10^{-7} Torr).

After setting up the anode–cathode bias to the designated field value, the probe was scanned in the *Y*-direction in steps of 50 μm and the field emission values were collected after allowing a brief settling time of 3–5 min. After completing one scan, the field value was brought to zero, the probe was moved to the starting *Y*-coordinate and the next *X*-location,

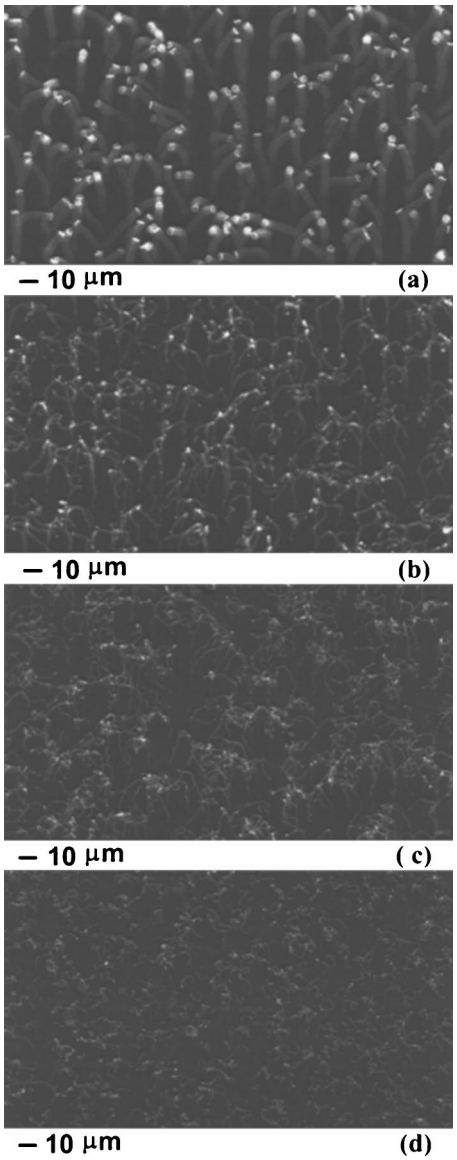

FIG. 2. SEM micrographs of carbon nanotube bundles of various diameter grown in arrays with 10 μm edge-to-edge bundle spacing. The bundles shown in (a)–(d) are of diameter 5 μm, 2 μm, 1 μm, and 0.5 μm, respectively. These micrographs show the degree of stiffness of CNT bundles as the bundle diameter decreases. The bundles droop significantly as the bundle diameter decreases.

and the scan was restarted as above. A total of three such measurement scans were performed on each sample.

III. RESULTS AND DISCUSSION

The results of field emission current as a function of nanotube bundle diameters and interbundle spacing are shown in Fig. 4. The turn-on voltage varied from 1.25 to 1.8 V/μm and the measurement field for the data shown was ~3 V/μm. The array layout is shown in the background of the emission curves to help identify the emission magnitude with the corresponding array.

As the probe was scanned, the emission current remained fairly constant at 0.8–0.9 μA across the 2 μm array, followed by >60× increase in the 5 μm array. The emission

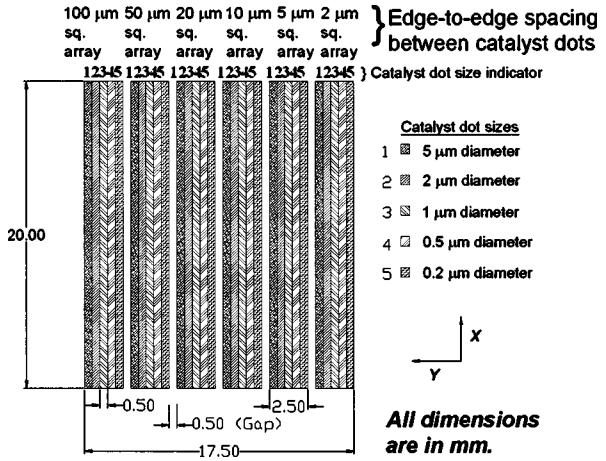

FIG. 3. Schematic of an array layout of dots of iron catalyst patterned by e-beam lithography, from which carbon nanotubes are grown.

decreased as the probe moved from the 5 μm array to the 10 μm array and decreased further by approximately three orders of magnitude in the 20 μm array. Almost no emission was recorded in the 50 μm and 100 μm arrays. The maximum current emission density observed in this scan was >0.6 A/cm^2 and this occurred in the 5 μm arrays of 1 μm and 2 μm bundle diameters. The emission behavior was reasonably consistent in the three scans at different *X*-locations on the sample, as can be seen in Fig. 4.

By driving these 5 μm—spacing, 1–2 μm—size bundle arrays to higher fields, we have been able to routinely achieve *1.5–1.8 A/cm^2 emission densities at ~4 V/μm* and with a lesser repeatability a current density of >6 A/cm^2 at 20 V/μm. These observed current densities at such low fields are much greater than the densities observed using either isolated single CNT (arranged in arrays with similar spacing) or dense mats of CNT grown from continuous Fe catalyst films. Our measurements on dense mats of CNT have shown emission in the order of 0.6–4 mA (densities in the range of tens to hundreds of mA/cm^2) between 4–6 V/μm,[18] while measurements on random arrays of

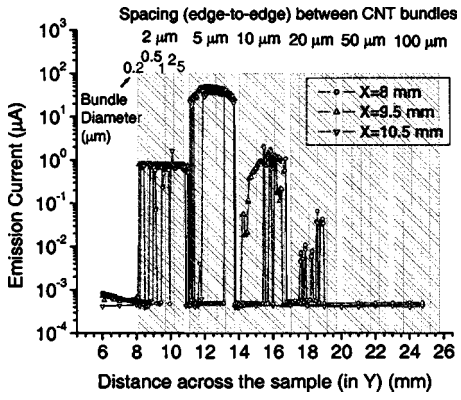

FIG. 4. Field emission current from arrays of nanotube bundles as a function of array spacing and bundle diameter measured as a probe anode is scanned across the arrays (three different curves indicate three different scanned locations). The topmost labels refer to edge-to-edge CNT bundle spacing.

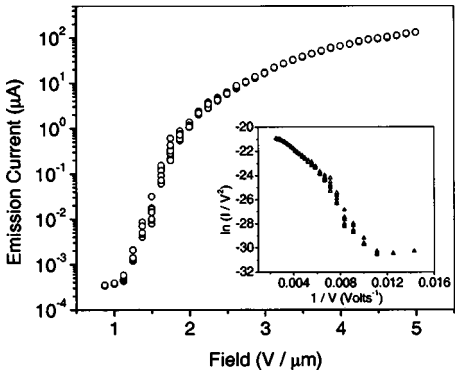

FIG. 5. Field-emission current vs voltage curve measured using 100-μm-diameter probe anode over 2-μm-diameter bundle arrays of 5 μm edge-to-edge spacing. The inset shows the corresponding Fowler–Nordeim curve.

CNT give current densities of $\sim$0.17 A/cm^2 to 1.4 A/cm^2 at fields of 6–10 V/μm. Among the previously published results of reported field emission current densities from CNT over measurement areas comparable to this work, only Zhu *et al.*[19] have reported current densities as high as 4 A/cm^2 over a (100 μm)^2 area and that data was taken at 60 V/μm. Figure 5 shows the field emission curve measured at the 2 μm bundle arrays of 5 μm spacing with the corresponding Fowler–Nordheim (F–N) (Ref. 20) curves in the inset. The calculated field enhancement factor was $\sim$4250.

Similar measurements were conducted with probe anode of diameter 200 μm, with a gap of 50 μm. The field emission pattern in this case was identical to that of 100-μm probe showing higher emission from 2 μm bundles in the 5 μm spaced arrays. In addition, this same pattern of field emission behavior (Fig. 4) was also observed for CNT bundle arrays grown directly on silicon substrates. From these measurements it seems the CNT bundles of 1–2 μm diameters with 5 μm edge-to-edge spacing offer an appropriate balance between emitter density and interemitter electrostatic shielding, giving rise to enhanced field emission when the area of field influence is $\geqslant$100 μm in diameter. Note that we can exclude the possibility that the observed differences in emission current are due to differences in nanotube length for various bundle sizes and spacings, because observed CNT bundle length was uniform throughout sample areas giving both low and high field emission. This is illustrated in Fig. 6, which shows CNT bundles with four different sets of size-spacing parameters. The CNT length is identical between these four sets of CNT bundles, while the field emission current yield under identical conditions from these sets spans two orders of magnitude (see Fig. 4).

The field emission pattern shown in Fig. 4 can be partly explained by the degree of stiffness of the bundles. The anode–cathode gap is set estimating the full height of the bundle under field influence. But, in larger spacing arrays ($>$20 μm edge-to-edge) because the bundles droop more (trend as shown in Fig. 1) the effective field seen by the bundles is lesser than that seen by the ones standing straight up. As a result, the emission current decreases when the

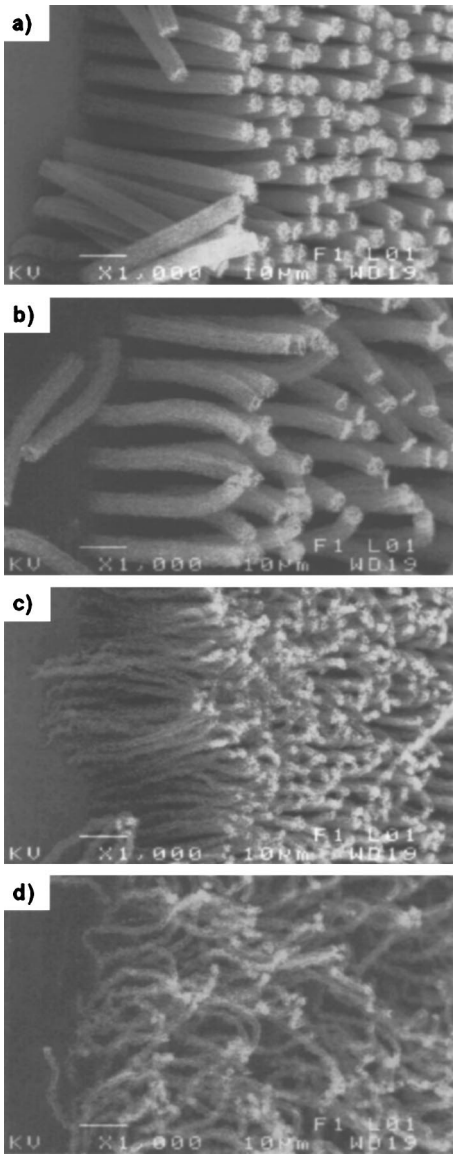

FIG. 6. SEM micrographs of carbon nanotube bundles of various diameter grown in arrays with various edge-to-edge bundle spacing. The bundles shown in (a)–(d) have diameter-separation parameters of 5 μm–2 μm, 5 μm–5 μm, 2 μm–2 μm, and 2 μm–5 μm, respectively. CNT bundles in all arrays have approximately the same length (height), however field emission current yield varies greatly between these bundle arrays.

probe scans over these arrays. Also, as mentioned before, the degree of stiffness of the bundles also depends on the bundle diameter—the thicker the bundle, the higher the stiffness (as shown in Fig. 2). Thus we see that in arrays of spacings 10 μm to 20 μm, the emission current increases as the bundle diameter increases, that is, as the bundles become stiffer (see Fig. 4). However, in 2 μm and 5 μm arrays the interbundle spacing is small enough to make all bundles stand straight up making the electric field seen by all of them effectively the same. For these arrays, we think the number density and the electrostatic screening play a dominant role in determining the emission current and, interestingly, we notice the emergence of an optimum bundle array architecture. While the bundles in 2 μm spaced arrays may experi-

ence higher screening, the total number density may be smaller in 10 μm spaced arrays. It appears that an optimum combination of these factors occurs at 1-μm and 2-μm-diameter bundles with 5 μm spacing, in that the 2-μm-diameter bundles have performed consistently well over different samples and scanning coordinates. It is difficult to directly correlate this optimum nature with the previously published criteria,[11,12] as the nanotube bundles are $\sim$50 μm tall and are spaced by only 5 μm edge-to-edge. It is possible that some rearrangement of individual tubes might be taking place at the top of these bundles, but it is not possible to substantiate it at this time.

IV. CONCLUSIONS

In summary, we have investigated the field emission performance of lithographically patterned arrays of carbon nanotube bundles and have found that these bundles perform dramatically better than either isolated CNT or dense mats of CNT. Among different array combinations tested, the bundles of diameter 1 μm and 2 μm, arranged in square arrays with 5 μm edge-to-edge spacing, produced the maximum emission when tested with $\geqslant$100-μm-diameter probe anodes. The bundles of 2 μm diameter gave the most consistent results between different scans and different samples. Using this setup, over a 100-μm-diameter area of field influence, we have consistently measured 1.5–1.8 A/cm^2 emission densities at fields as low as 4 V/μm, and $>$6 A/cm^2 has been observed at a 20 V/μm field. These bundles in optimum array geometry are suitable for applications requiring integration of extraction grid and other beam focusing electrodes because of their free-standing geometry.

ACKNOWLEDGMENTS

This research was carried out at the Jet Propulsion Laboratory, California Institute of Technology, under a contract with National Aeronautics and Space Administration (NASA). This work was funded by NASA's Code-R grants and JPL's Director's Research and Development Fund. The Authors would like to thank Dr. Johan Backlund, Dr. Daniel Wilson, Dr. Richard Mueller, and Dr. Pierre Echternach of JPL for their assistance with the electron beam lithography and Peter J. Bruneau of JPL for precision machining of components of the experiment set-up.

[1]A. A. Talin, K. A. Dean, and J. E. Jaskie, Solid-State Electron. **45**, 963 (2001).
[2]J. M. Bonard, H. Kind, T. Stöckli, and L. Nilsson, Solid-State Electron. **45**, 893 (2001).
[3]H. Murakami, M. Hirakawa, C. Tanaka, and H. Yamakawa, Appl. Phys. Lett. **76**, 1776 (2000).
[4]W. Zhu, C. Bower, G. P. Kochankski, and S. Jin, Solid-State Electron. **45**, 921 (2001).
[5]P. H. Siegel, T. H. Lee, and J. Xu, JPL New Technology Report, NPO 21014, March 21, 2000.
[6]P. H. Siegel, A. Fung, H. M. Manohara, J. Xu, and B. Chang, in Proceedings of the 12th International Symposium on Space Terahertz Technology 2001, Jet Propulsion Laboratory, San Diego, CA, pp. 94–103.
[7]J. T. L. Thong, C. H. Oon, W. K. Eng, W. D. Zhang, and L. M. Gan, Appl. Phys. Lett. **79**, 2811 (2001).
[8]J. I. Sohn, S. Lee, Y. H. Song, S. Y. Choi, K. I. Cho, and K. S. Nam, Appl. Phys. Lett. **78**, 901 (2001).
[9]A. M. Rao, D. Jacques, R. C. Haddon, W. Zhu, C. Bower, and S. Jin, Appl. Phys. Lett. **76**, 3813 (2000).
[10]S. Fan, M. G. Chapline, N. R. Franklin, T. W. Tombler, A. M. Cassell, and H. Dai, Science **283**, 512 (1999).
[11]L. Nilsson, O. Groening, C. Emmenegger, O. Kuettel, E. Schaller, L. Schlapbach, H. Kind, J.-M. Bonard, and K. Kern, Appl. Phys. Lett. **76**, 2071 (2000).
[12]J. S. Suh, K. S. Jeong, J. S. Lee, and I. Han, Appl. Phys. Lett. **80**, 2392 (2002).
[13]V. I. Merkulov, D. H. Lowndes, and L. R. Baylor, Appl. Phys. Lett. **89**, 1933 (2001).
[14]M. Chhowalla, C. Ducati, N. L. Rupesinghe, K. B. K. Teo, and G. A. J. Amaratunga, Appl. Phys. Lett. **79**, 2079 (2001).
[15]V. Semet, V. T. Binh, P. Vincent, D. Guillot, K. B. K. Teo, M. Chhowalla, G. A. J. Amaratunga, W. I. Milne, P. Legagneux, and D. Pribat, Appl. Phys. Lett. **81**, 343 (2002).
[16]S. H. Jo, Y. Tu, Z. P. Huang, D. L. Carnahan, D. Z. Wang, and Z. F. Ren, Appl. Phys. Lett. **82**, 3520 (2003).
[17]K. B. K. Teo, M. Chhowalla, G. A. J. Amaratunga, W. I. Milne, G. Pirio, P. Legagneux, F. Wyczisk, D. Pribat, and D. G. Hasko, Appl. Phys. Lett. **80**, 2011 (2002).
[18]H. M. Manohara, W. Dang, M. Hoenk, A. Husain, P. H. Siegel, and A. Scherer, Proc. SPIE **5343**, 227 (2004).
[19]W. Zhu, C. Bower, O. Zhou, G. Kochanski, and S. Jin, Appl. Phys. Lett. **75**, 873 (1999).
[20]R. H. Fowler and L. W. Nordheim, Proc. R. Soc. London, Ser. A **119**, 173 (1928).